Influences of Nano-sized Crystalline Particles on the Mechanical Properties of Metallic Glass – A Molecular Dynamics Study –

R. Matsumoto[1], N. Miyazaki[1] and M. Nakagaki[2]

Summary

The mechanical properties of amorphous metals and metallic glasses are remarkably changed by precipitated crystalline particles. In this paper, the effects of crystal particle size and volume fraction on the flow stress of the metallic glass are evaluated by molecular dynamics simulations. The investigated volume fraction ranges from 0 % (metallic glass) to 100 % (nanocrystalline metal), and the average particle diameter ranges from 1nm to 12nm. It is revealed that the dispersed particle effects on the flow stress are very small in the entire volume fraction range when the average particle diameter is smaller than 3 nm, and the flow stress is intensified as the particle size increases until about 6 nm. For a larger particle size (d >6 nm), the flow stress is not influenced by the particle size, when the crystal volume fraction is lower than 60 %, and the particle size effects appear gradually for the higher crystal volume fraction (d >60 %). It is shown that this phenomenon is caused by the increase of the fraction of grain boundary to the entire interface.

Introduction

The mechanical properties such as elastic constants and flow stress of amorphous metals and metallic glasses are changed remarkably by the precipitated crystalline particles [1]∼ [3]. In order to give a definite guide to develop new materials composed of amorphous and crystal phases with desired properties, it is important to reveal the relationship between the internal structures and the mechanical properties of the metallic glasses containing nano-sized crystalline particles. However, there have not been enough analysis of the particle size and crystal volume fraction effects on the mechanical properties and deformation behaviors of metallic glasses. In this paper, the particle size effects on the flow stress are estimated through all crystal volume fraction from 0 % (amorphous) to 100 % (nanocrystalline metal) by molecular dynamics simulations of tensile deformation of model metallic glasses with dispersed nano-sized crystalline particles. .

Model and Simulation Method

In this study, the Parrinello-Pahman's algorithm [4][5] is used to control the external stress, and the velocity scaling method is also used to control the temperature. The periodic boundary condition to the x, y, z-axis is also applied in all the

---

[1]Department of Mechanical Engineering and Science, Graduate School of Engineering, Kyoto University

[2]Trustee, Kyushu Institute of Technology

following simulations . The domain decomposition method for parallel calculation and the link-cell method are used in order to perform large-scale simulations. The Lennard-Jones potential, modified to enforce the continuity at the cut off distance, was used as an interatomic potential. Inoue's three basic principles to generate bulk metallic glass [6] were used to define the potential parameters. The parameters are shown in Table 1. In the table, σ and ε are potential parameters that determine the equilibrium interatomic distance and binding energy, respectively. The binding energy parameter is $\varepsilon = 0.6 \times 10^{-19}$ J for the same kind of atoms ('a-a', 'b-b' and 'c-c'), and $\varepsilon = 0.65 \times 10^{-19}$ J for the different kinds of atoms. The interatomic distance parameter σ is averaged when the interacting atoms are different.

Table 1: Potential parameters

Kind of atom	a	b	c
σ [nm]	0.25	0.3	0.35
ε [10^{-19}J]	0.6		
r_c [nm]	0.786		
m [10^{-25} Kg]	0.5787	1.000	1.5880

In this paper, simulation models containing enough crystal particles to present isotropic properties are treated. We used the following process for our analysis model (see Fig. 1). Two dimensional schematic views are used for simple description in Fig.1(i), (ii) and (iii).

1. Formation of amorphous blocks

   Cubic blocks with an amorphous structure were numerically produced by the melting-rapid quenching simulation [7] [8].

2. Definition of particle positions (see Fig. 1(i))

   First, each edge of the amorphous blocks are divide into n sections; *i.e.*, the blocks are divided into n^3 cubes with the same size, and then the initial particle-centers are arranged at the each center of the face and each vertex of the cube. Then, each initial particle-center is moved randomly in the spherical region with radius $e \times h$, it is shown in the figure by the circles drawn in dotted lines. Here, h is the distance between initial particle-centers; *i.e.* $h = L_0/n/\sqrt{2}$. $n = 2$ and $e = 0.5$ are respectively used in this research, therefore a unit cell contains 32 crystal particles. In this paper, the particle-centers were arranged at the relatively same positions in a unit cell for all simulation models.

3. Making space to introduce crystal particles (see Fig. 1(ii))

   Spherical areas with radius $d_0/2$ centered at the crystal-centers defined in the previous proceedure are cut out from each amorphous block.

4. Introduction of crystalline particles into the amorphous block (see Fig. 1(iii))

   Crystal particles made of element 'b' with radius $d_0/2$ are introduced into the hollowed areas. The crystal orientation of each particle was defined in a random manner. If crystal particles are overlapped each other, the domains are divided by the Voronoi's division. In other words, when the distance between particle-centers d_p is closer than the initial particle diameter d_0, there exists grain boundary in the mid-plane of the particle-centers. In this paper, the crystal orientations are also defined to be the same in all models.

5. Elimination of atomic pairs that are too close together

   Since the crystalline particles were artificially introduced into the amorphous blocks in the previous procedure, the interatomic distance between some of the atomic pairs near the amorphous-crystal interface was too close. One atom of each of these pairs was removed randomly because such pairs caused problems at the beginning of the simulation. In this research, 0.73 times the equilibrium interatomic distance of the pair was chosen as a critical distance.

6. Relaxation and tensile deformation simulation (see Fig. 1(iv))

   For simulation models with very small particle size ($d \leq 4$ nm), the unit cell was periodically arranged in one calculation cell in order to reduce the difference of number of atoms. And then, the relaxation calculations were performed during 20 ps under constant stress $\bar{\sigma}_x = \bar{\sigma}_y = \bar{\sigma}_z = -0.1$ MPa and constant temperature $T = 300$ K. And then loading simulations were performed. During the loading simulations, the cell length L_y was stretched by strain-rate $\dot{\varepsilon}_y$ under $T = 300$ K and $\bar{\sigma}_x = \bar{\sigma}_z = -0.1$ MPa. Here, the rate of true strain was used for the strain rate. In Fig.1(iv), only crystal phase are displayed and they are colored by the lattice orientation in order to distinguish each particle.

   34 simulation models are described in this paper. Simulation conditions are shown in Fig.2. Here, f is the crystal volume fraction, and d is the averaged particle diameter after the Voronoi's division.

Result and Discussions

   Figure 3 shows the relationship between the crystal volume fraction f and the flow stress σ_f. Here, the flow stresses were obtained from the averaged stress during $\varepsilon_y = 0.25 \sim 0.48$. The dispersed particle effects on the flow stress are very small in the entire volume fraction range when the average particle diameter is smaller than 3 nm. This size is very close to the size of shear transformation zone (STZ) in the metallic glass. And the flow stress is intensified as the particle size increases until about 6 nm. For a larger particle size ($d >6$ nm), the flow stress is not influenced by the particle size, when the crystal volume fraction is lower than 60 %,

Unit amorphous block

(i) Step 2

Amorphous phase
Hollowed area

(ii) Step 3

$\dot{\varepsilon}_y$

Crystal phase

Crystal orientation
Grain boundary

(iii) Step 4
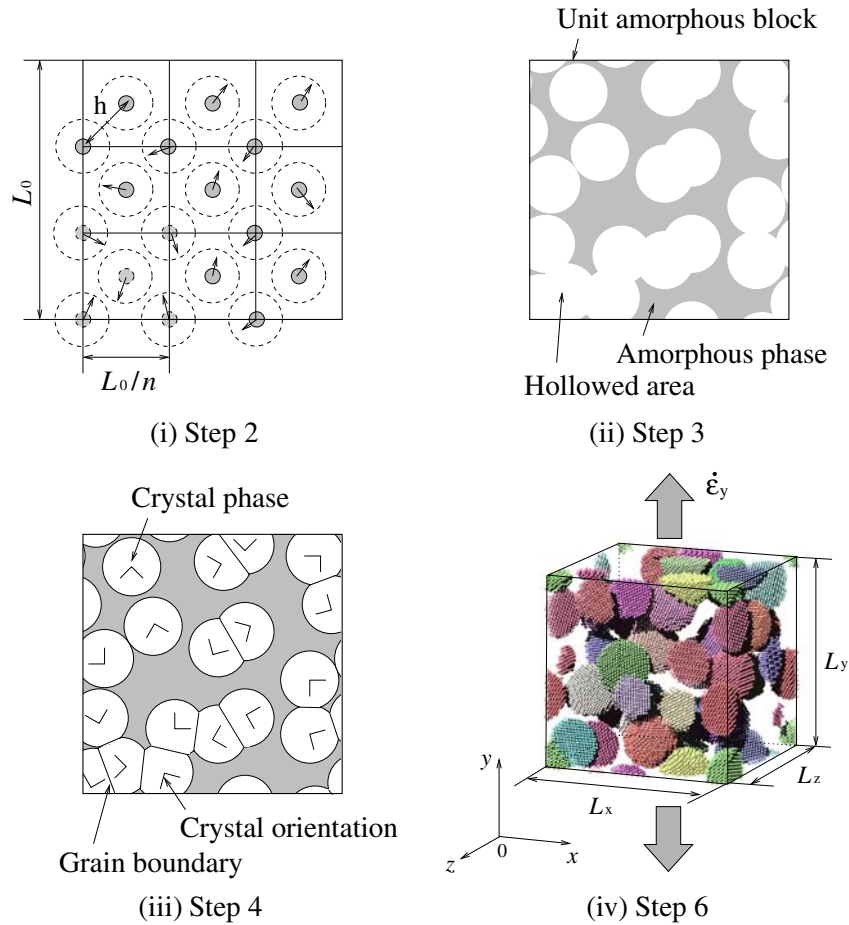
L_y

L_z

L_x

(iv) Step 6

Figure 1: Simulation model

and the particle size effects appear gradually for the higher crystal volume fraction ($d > 60\%$).

Figure 4 shows the flow stress σ_f , the averaged stress in the crystal phase σ_{f-cry} and the amorphous phase σ_{f-amo} for $d_0 = 6$ nm and $d_0 = 12$ nm. From Fig. 4, it is found that σ_{f-cry} increases until $f \simeq 30\%$, and then it keeps almost constant value for a while. σ_{f-cry} reaches the yield stress around $f \simeq 30\%$ and particles begin to undergo deformations remarkably, therefore the increase of σ_{f-cry} is limited. We have reported in the previous paper [8] that the amorphous-crystal interface rarely cause stress concentration, and consequently crystal particles in the amorphous phase have high yield stress. However, the high crystal volume fraction models contain grain boundaries and also contain triple junctions of grain
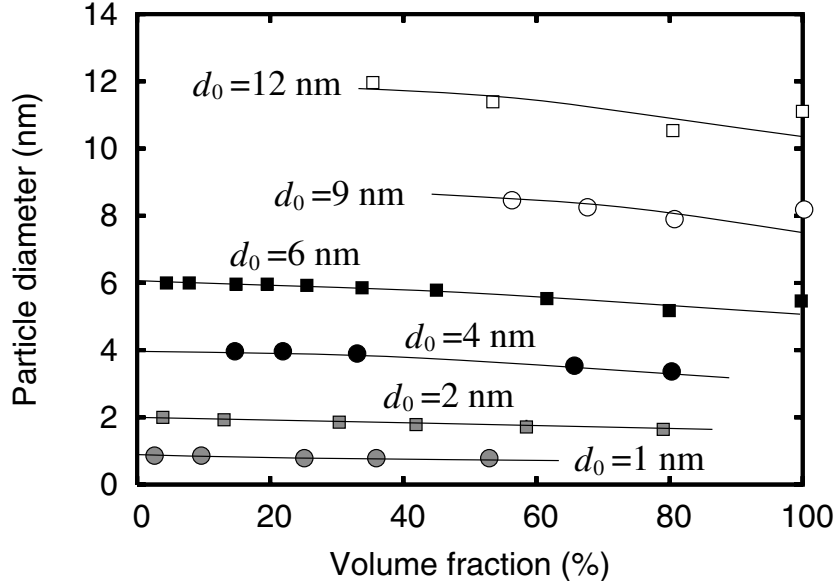
Figure 2: Simulation conditions

boundaries, and they can become the origination points of deformations. Therefore, σ_{f-cry} is decreased for high crystal volume fraction models ($f > 60$ %). Here, we have to notice that the fraction of the grain boundary to the entire interface increases drastically for $f > 60$ %, while it is almost 0 % for the low crystal volume fraction models. On the other hand, σ_{f-amo} is almost constant except high volume fraction models. From the above discussion, the flow stress of the composite σ_f ($= f\sigma_{f-cry} + (1 - f)\sigma_{f-amo}$) is increased with increasing the slope for the small crystal volume fraction, because σ_{f-cry} and f increase. And then, σ_{f-cry} increases linearly until $f \simeq 60$ %, because the averaged stress in the crystal phase σ_{f-cry} and the amorphous phase σ_{f-amo} becomes almost constant. We have reported that dislocations can across the amorphous-crystal interface easily without pile up [8]. However, most grain boundaries have large resistance to dislocation motions, therefore the particle size effects appear gradually for the higher crystal volume fraction.

Conclusions

In this research, the particle size and volume fraction effects on the flow stress are estimated through 0% (amorphous) to 100% (nanocrystalline metal) by molecular dynamics simulations. It is revealed that the dispersed particle effects on the flow stress are very small when the average particle diameter is smaller than 3 nm, and the flow stress is intensified as the particle size increases until about 6 nm. This phenomenon may relevant to the size of shear transformation zone in the metallic
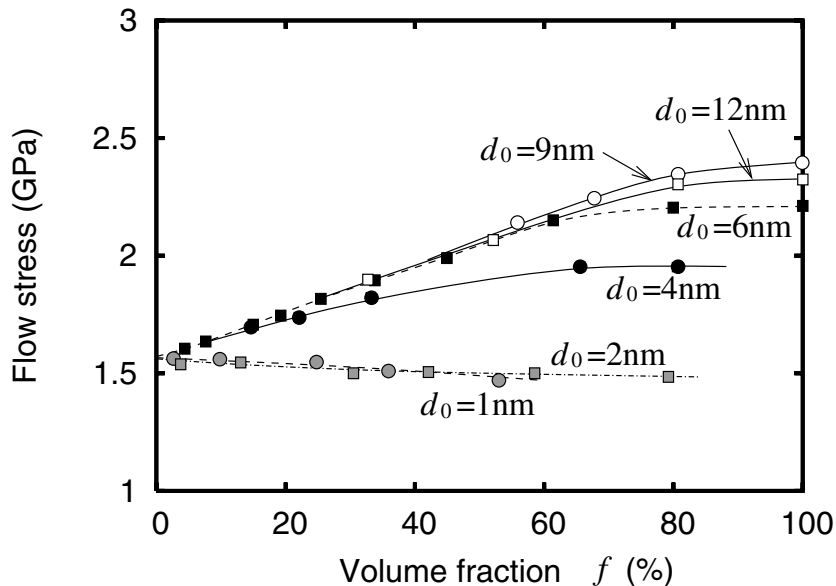
Figure 3: Influence of the crystal volume fraction f and particle diameter d on the flow stress σ_f

glass. For a larger particle size ($d > 6$ nm), the flow stress is not influenced by the particle size, when the crystal volume fraction is lower than 60 %, and the particle size effects appear gradually for the higher crystal volume fraction ($d > 60$ %). It is shown that this phenomenon is caused by the increase of the fraction of the grain boundary to the entire interface.

References

1. Jiang, X. Y. *et al.*, *Mat. Sci. & Eng., A*, **226-228** (1997), 789-793.

2. Kim, T.S. *et al.*, *Mat. Sci. & Eng., A*, **363** (2003), 81-85.

3. Matsumoto, R., Nakagaki, M., Nakatani, A. and Kitagawa, H., *CMES*, **9**-1 (2005), pp.75-84.

4. Parrinello, M. and Rahman, A., *Phys. Rev. Let.*, **45**-14 (1980), 1196-1199.
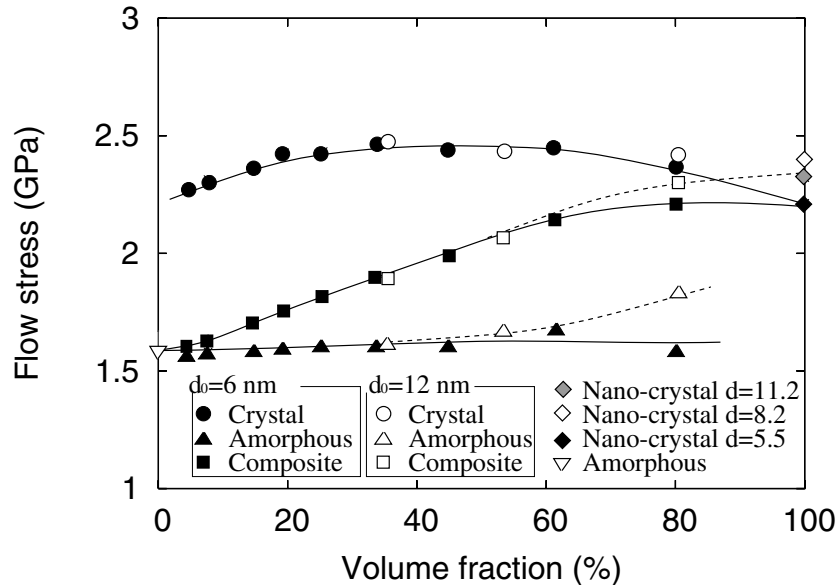
Figure 4: Influence of the crystal volume fraction f and particle diameter d on the flow stress σ_f, stress averaged in cyrstalline phase σ_{cry} and amorphous phase σ_{amo}

5. Parrinello, M. and Rahman, A., *J. Appl. Phys.*, **52**-12 (1981), 7812-7190.

6. Inoue, A., *Acta Mater.*, **48** (2000), 279-306.

7. Nakatani, K. *et al.*, *AIAA Journal*, **38**-4 (2000), 695-701.

8. Matsumoto, R. and Nakagaki, M., (2005), *CMES*, **10**-3 (2005), pp.187-199.